THE JOURNAL OF PHYSICAL CHEMISTRY C

Article

pubs.acs.org/JPCC

How Oxygen Vacancies Activate CO_2 Dissociation on TiO_2 Anatase (001)

Stijn Huygh, Annemie Bogaerts, and Erik C. Neyts*

Research Group PLASMANT, Department of Chemistry, University of Antwerp, Universiteitsplein 1, B-2610 Antwerp, Belgium

ABSTRACT: The adsorption, dissociation, and diffusion of CO_2 on the anatase (001) surface was studied using DFT by means of the generalized gradient approximation using the Perdew–Burcke–Ernzerhof (PBE)-functional and applying corrections for long-range dispersion interactions. Different stable adsorption configurations were identified for the fully oxidized surface. The most stable adsorption configuration is the monodentated carbonate-like structure. Small energy barriers were identified for the conversion of a physisorbed to a chemisorbed configuration. CO_2 dissociation is found to be unfeasible on the stoichiometric surface. The introduction of oxygen vacancy defects gives rise to new highly stable adsorption configurations with a stronger activation of the C–O bonds. This leads to the possibility of exothermic dissociation of CO_2 with barriers up to 22.2 kcal/mol, corresponding to chemical lifetimes of less than 4 s at 300 K. These reactions cause a CO molecule to be formed, which will easily desorb, and the reduced surface to become oxidized. It is clear that oxygen vacancy defects play a key role in the catalytic activity of an anatase (001) surface. Oxygen vacancies play an important role in the dissociation of CO_2 on the anatase (001) surface, and will play a significant role in complex problems, such as the catalytic conversion of CO_2 to value-added chemicals.

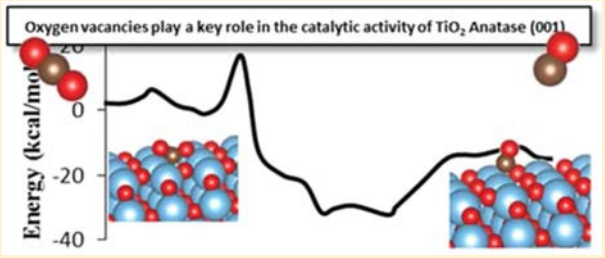

1. INTRODUCTION

One of the major concerns of the current era is global climate change. The intergovernmental panel on climate change reported in 2014 that each decade in the last 30 years has been successively warmer than any other since 1850.[1] It is generally agreed upon that the main cause of global warming is the anthropogenic extension of the greenhouse effect by emission of greenhouse gases such as CO_2.[1−4] The global CO_2 concentration has surpassed the 400 ppm mark in March 2015 for the first time since the measurements began.[5]

There exist several strategies to decrease the concentration of CO_2 in the atmosphere, in order to mitigate the effect of greenhouse gases on the global climate. The first and most obvious strategy is the reduction of the CO_2 emission itself with the use of CO_2 neutral energetic technologies (photovoltaics, wind energy, biogas, etc.). However, it will be difficult to decrease the concentration of CO_2 by this strategy alone, as the global population will keep increasing and economies will further develop. To achieve a strong reduction in the global CO_2 concentration, this strategy could be combined with the conversion to added-value chemicals. Among other techniques, including, e.g., plasma conversion,[6−13] heterogeneous catalysis on reactive metal and metal oxide surfaces is a viable route.[14] Indeed, this approach combines a mitigation of the greenhouse effect with the chemical conversion of CO_2 to useful chemicals.

In 1979 Inoue and co-workers reported that the aqueous suspension of a semiconductor (TiO_2, ZnO, CdS, etc.) can photoreduce CO_2 to form formic acid, formaldehyde, methanol, and methane.[15] Among the various catalysts reported in that paper, TiO_2 is often used as a model system for the catalytic properties of metal oxides.

To improve the performance of catalytic processes on TiO_2, it is important to get a better fundamental insight into the adsorption and activation of CO_2 on TiO_2 surfaces. In this work we study the interaction of CO_2 with anatase (001), and more specifically the influence of oxygen vacancies on the adsorption and activation of CO_2. In the study of Yu et al. it is found that the photocatalytic reduction of CO_2 on anatase is strongly influenced by the ratio of (101) and (001) facets in the crystal.[16] They found that the sample with 58% (001) facet has the highest reactivity for the photocatalytic reduction of CO_2. Also, a higher methane production was reported for samples consisting of mostly the (001) facet than for the samples consisting of mostly the (101) facet. For other small molecules it is suggested that the (001) facet has a higher reactivity compared to the most stable (101) facet.[17,18] Mino et al. performed combined FTIR and DFT studies of the adsorption of CO and CO_2 on TiO_2 anatase surfaces and found that the surface Ti sites present at the (001) facet have a lower Lewis acidity than the Ti sites at the (101) facet, and the surface oxygen sites exhibit a stronger Lewis basicity on anatase (001) than on the anatase (101) surface.[19,20] This strongly influences the adsorption of CO_2 on anatase. CO_2 is mainly adsorbed in linear form on the anatase (101) surface with an adsorption energy of −11.1 kcal/mol, as the carbonate-like adsorption configuration has an adsorption energy of only −3.7 kcal/mol,[21] while on the anatase (001) surface CO_2 adsorbs mostly in a carbonate-like structure with an adsorption energy of −30.1

Received: July 25, 2016
Revised: August 31, 2016
Published: September 2, 2016

DOI: 10.1021/acs.jpcc.6b07459
J. Phys. Chem. C 2016, 120, 21659−21669

kcal/mol and the linear configuration only has an adsorption energy of −5.3 kcal/mol.[20]

Apart from the inherent difference in Lewis acidity and basicity of the surfaces, it is possible to increase the Lewis basicity of the surface by introduction of oxygen vacancies.[22] Sorescu et al. found that oxygen vacancies significantly influence the adsorption properties of CO_2 on rutile (110) and anatase (101) surfaces, and they anticipated that these defects play an important role in the complex surface chemistry of CO_2 catalysis.[21,23] Previous studies have also shown a significant influence of the presence of oxygen vacancies on the adsorption properties of H_2O, O_2, and methane derived radicals.[24−27] Barzan et al. have shown the unprecedented potential of TiO_2 samples reduced in a H_2 atmosphere in the conversion of ethylene to high density polyethylene under mild conditions and without any activator.[28] It is shown that reduced TiO_2 always has a higher catalytic activity for the reduction of CO_2, as the presence of point defects provides more active sites.[29] The presence of Ti^{3+} generated by the presence of oxygen vacancies is suggested to facilitate CO_2 reduction.[30] The intrinsic defects can act as initiators and activators for heterogeneous catalysis. Understanding the influence of oxygen vacancies on the adsorption and reactions of CO_2 on TiO_2 is thus key for a fundamental understanding of the catalytic activity of TiO_2. As the position of the defects determines the surface chemistry, we here study the adsorption and dissociation of CO_2 on anatase (001) surfaces containing one of the three most stable oxygen vacancies.[27] For anatase (101) it has been shown experimentally[31] and suggested by simulations[32,33] that oxygen vacancies diffuse easily even at room temperature; therefore, we expect that the same is true for anatase (001). This means that the different oxygen vacancies will all be accessible for reactions and adsorption.

2. COMPUTATIONAL DETAILS

The calculations were performed using the Vienna ab initio simulation package (VASP).[34,35] For the treatment of the exchange and correlation, the Perdew−Burke−Ernzerhof (PBE) functional was applied,[36] using plane wave basis sets and the projector-augmented wave method[37] as implemented in VASP. It has been shown by Sorescu et al. that long-range dispersion interactions play an important role in the interactions of CO_2 with TiO_2.[21] Therefore, we have corrected the PBE functional with long-range dispersion interactions by applying the Tkatchenko and Scheffler method[38] as recently implemented in VASP.[39]

The stoichiometric anatase (001) surface was modeled using a (2 × 2) supercell containing 48 atoms corresponding to four TiO_2 layers. We fixed the bottom layer of the surface at the bulk positions and expanded the simulation box to create a vacuum layer of ∼16 Å between adjacent surfaces to prevent the influence of neighboring slabs on the adsorption properties. An energy cutoff of 440 eV was used, and the sampling of the Brillouin zone was performed using 6 × 6 × 1 k-points for the surface models and only the gamma-point for the CO_2 and CO molecules. Geometry optimizations were performed with the end point criterion of the residual forces to be below 0.03 eV·$Å^{-1}$. Spin polarization was applied for all calculations.

The vibrational analysis was performed with the finite difference method implemented in VASP. Two sets of calculations were performed for the vibrational analysis. In the first set of calculations that were preformed, the finite difference displacements were only applied to the CO_2 molecule. The resulting frequencies were reported as the vibrational frequencies of the adsorbed molecule. The second set of calculations included the displacements to both the CO_2 molecule and the top layer of the TiO_2 surface. These results were used for the thermodynamical analysis as performed with the TAMKIN tool.[40]

The adsorption energy of CO_2 on the stoichiometric and reduced surfaces is calculated as follows:

$$E_{ads} = E_{CO2+surface} - E_{CO2} - E_{surface}$$

where E_{CO2} is the total energy of the optimized gas phase CO_2 molecule with zero-point energy corrections included, $E_{surface}$ is the total energy of the respective surface with zero-point energy corrections, and $E_{CO2+surface}$ is the total energy of the respective surface with CO_2 adsorbed with zero-point energy corrections.

The extent of charge transfer from the surface to the adsorbed CO_2 molecule was calculated using Hirshfeld charges.[41] To study the adsorption mechanism and the effect of the oxygen vacancies on the activation barrier of CO_2 reduction, we calculated the corresponding minimum energy barriers with Nudged Elastic Band (NEB)[42−47] as implemented in the VASP code.

3. RESULTS AND DISCUSSION

3.1. CO_2 Adsorption on the Oxidized (Nondefective) Anatase (001) Surface. We identified different binding configurations of CO_2 on the stoichiometric surface, of which a pictorial view is shown in Figure 1. The relevant bond lengths, bond angles, adsorption energies, vibrational frequencies, and charge transfer are given in Table 1. The first and most stable configuration is a monodentate carbonate-like structure, B(I). In this configuration, CO_2 binds with its oxygen atoms to two 5-fold coordinated Ti(5f) centers in the same [010] row, and with its carbon atom to the 2-fold coordinated oxygen (O(2f)) center of the Ti−O(2f)-Ti bridge. The O−C−O bond angle is 129.9°. This configuration has a strong exothermic adsorption energy of −32.8 kcal/mol, despite the energy cost of bending the CO_2 from its linear gas phase configuration to the bent configuration and the significant deformation of the anatase surface. The O(2f), participating in the monodentated carbonate-like structure, is displaced inward by 0.8 Å, and the Ti−O(2f)-Ti angle changes from 155.2° to 179.2°. This structure has previously been reported by Mino, Indrakanti, and

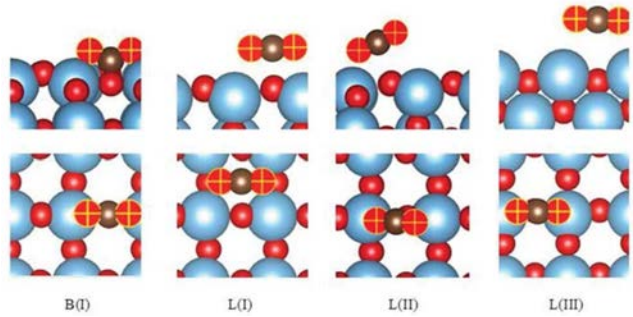

Figure 1. Different adsorption configurations of CO_2 on the stoichiometric anatase (001) surface, in side view and top view (upper and lower panels, respectively). Ti = blue, O_{TiO2} = red, O_{CO2} = red with yellow plus sign, C = brown. B(I) is a strong chemisorbed monodentate carbonate configuration, while L(I), L(II), and L(III) are physisorbed configurations.

DOI: 10.1021/acs.jpcc.6b07459
J. Phys. Chem. C 2016, 120, 21659−21669

Table 1. Adsorption Properties of CO_2 on a Stoichiometric TiO_2 Anatase (001), for the Gas Phase, Chemisorbed (B(I)), and Several Physisorbed (L(I), L(II), L(III)) Configurations[a]

Configuration	r(Ti−O_{CO2}) (Å)	r(O_{surf}−C) (Å)	r(C−O_{CO2}) (Å)	α(OCO) (deg)	E_{ads} (kcal/mol)	$\upsilon(CO_2)$ (cm^{-1})				$\Delta q(CO_2)$ (a.u.)	E_a (kcal/mol)
Gas phase			1.177, 1.177	180.0		2365	1316	632	631		
B(I)	2.073, 2.088	1.323	1.284, 1.280	129.9	−32.82	1558	1313	844	751	−0.214	30.42
L(I)		2.956, 2.924	1.177, 1.177	177.7	−7.31	2356	1315	615	613	0.066	0.80
L(II)	2.460	2.514	1.187, 1.170	173.5	−6.19	2344	1304	622	566	0.104	0.20
L(III)	3.089, 3.249		1.177, 1.176	179.7	−4.34	2358	1317	634	620	0.098	0.26

[a]The bond lengths between Ti and O of CO_2, r(Ti−O_{CO2}), between the surface O and C, r(O_{surf}−C), and between C and O of CO_2, r(C−O_{CO2}), the bond angle of CO_2, α(OCO), the adsorption energy, vibrational frequencies $\upsilon(CO_2)$, the charge transfer from the surface to CO_2, $\Delta q(CO_2)$, and the activation energy for diffusion to a B(I) adsorption configuration E_a.

Pipornpong, with adsorption energies ranging from −30.1 to −26.2 kcal/mol.[20,48,49] However, they did not include zero point energy corrections nor long-range dispersion corrections.

Mino et al. reported IR frequencies for the monodentated carbonate configuration of 1587 and 1316 cm^{-1} for spectra taken at room temperature of CO_2 adsorbed on TiO_2 anatase nanopowder outgassed at 823 K to remove residual coadsorbed water and fully oxidized by exposure to O_2 at 723 K.[20] These values correspond well with the values obtained in our calculation, viz. 1558 and 1313 cm^{-1}, respectively. The increasing C−O bond length (from 1.18 Å in the gas phase to 1.28 Å in the B(I) configuration), the strong red shift of the asymmetric stretch (from 2365 to 1558 cm^{-1}), and the significant charge transfer to CO_2 (−0.214 au) as resulting from the adsorption, all suggest an activation of CO_2 for the reduction of CO_2. However, as shown by Pipornpong et al., dissociative adsorption of CO_2 on a fully oxidized anatase (001) surface has an unfavorable adsorption energy of 76.2 kcal/mol.[49] In comparison, we find a similar dissociative adsorption energy of 67.4 kcal/mol and a dissociation energy barrier of 113.6 kcal/mol, as will be shown later. It is thus clear that CO_2 dissociation on the fully oxidized surface will not occur without the help of coadsorbates that stabilize the transition state and the reaction products, i.e., CO and atomic oxygen adsorbed on the fully oxidized surface.

Apart from the strong chemisorbed monodentate carbonate configuration, there exist several physisorbed configurations, which form shallow metastable intermediates upon adsorption of CO_2 from the gas phase (see configurations L(I), L(II), and L(III) in Figure 1). In particular, when CO_2 undergoes physisorption, it will subsequently convert to the B(I) configurations over low energy barrier pathways. These barriers range from 0.2 to 0.8 kcal/mol, and hence the conversion from any of the physisorbed configurations to the B(I) chemisorbed configuration will easily occur, even at room temperature. However, diffusion from one chemisorbed configuration to a neighboring adsorption site requires crossing an energy barrier of 30.4 kcal/mol, which is not easily accessible at low temperatures. As this barrier is comparable to the desorption energy of 32.8 kcal/mol, desorption and diffusion will be competitive at elevated temperatures.

3.2. CO_2 Adsorption on a Reduced (Defective) Anatase (001) Surface. As mentioned in the introduction, the behavior of reactive species under the influence of oxygen vacancies present in TiO_2 is a key factor in its catalytic activity. In our previous work we determined the formation energy of different oxygen vacancies in anatase (001).[27] The position of the different oxygen vacancies is shown in Figure 2. The formation energies for V_{O1}, V_{O2}, V_{O3}, and V_{O4} are 102.9, 115.0, 110.8, and 132.7 kcal/mol, respectively.[27] We will only investigate the influence of V_{O1}, V_{O2}, and V_{O3}, as V_{O4} is too unstable to have a significant influence on the adsorption of CO_2.

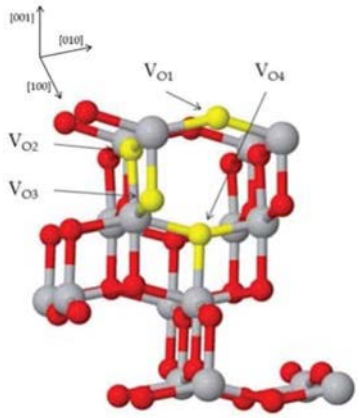

Figure 2. . Different oxygen vacancies in an anatase (001) TiO_2 surface. (Ti = gray, O = red, oxygen vacancy = yellow.)

3.2.1. CO_2 Adsorption near an Oxygen Vacancy. In this section, we investigate the influence of the presence of different oxygen vacancies on the adsorption properties of the stable adsorption configurations found on the fully oxidized surface. The adsorption energies of CO_2 on the oxygen vacancy containing surface as well as the original adsorption strengths (i.e., on the fully oxidized surface) are shown in Figure 3. In panel a, site 0 corresponds to the stoichiometric configuration (i.e., without an oxygen vacancy present in the surface). Sites 1 and 2 correspond to an oxygen vacancy present closest to the adsorbed CO_2, and the vacancy present on the position of the neighboring O(2f) in the same [010] row (see Figure 2) of the stoichiometric surface, respectively. Sites 3 and 4 are equivalent to sites 1 and 2, respectively, but in the neighboring [010] row. In panel b, site 0 corresponds to the configuration on the stoichiometric surface and site 1 corresponds to the oxygen vacancy present closest to the adsorbed CO_2 molecule. For B(I), site 2 is equivalent to site 1, as the removal of any of the V_{O2} oxygen atoms will result in the same adsorption configuration due to symmetry. For L(I), the oxygen vacancy is located in the parallel [010] row, and for L(II) and L(III), the oxygen vacancy is located in the parallel [100] row. In panel c, site 0 corresponds to the configuration on the stoichiometric surface. Sites 1 and 2 correspond to the V_{O3} oxygen vacancy present closest to the adsorbed CO_2 and the vacancy present in the same [010] row of the neighboring [100] row, respectively.

DOI: 10.1021/acs.jpcc.6b07459
J. Phys. Chem. C 2016, 120, 21659−21669

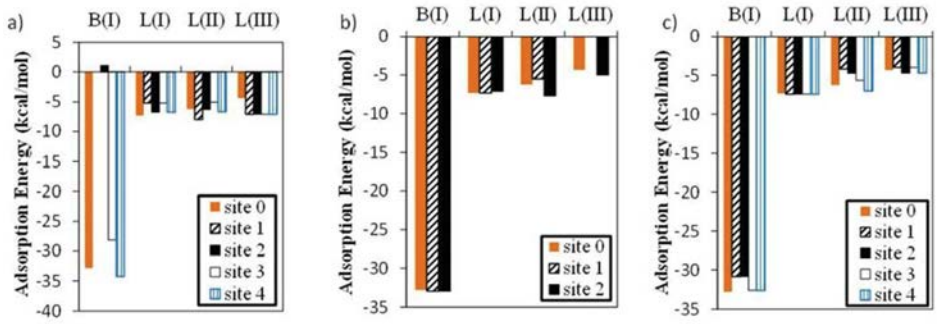

Figure 3. Adsorption energy of the adsorption configurations of CO_2 on a reduced anatase (001) surface with a (a) V_{O1} vacancy, (b) V_{O2} vacancy, or (c) V_{O3} vacancy.

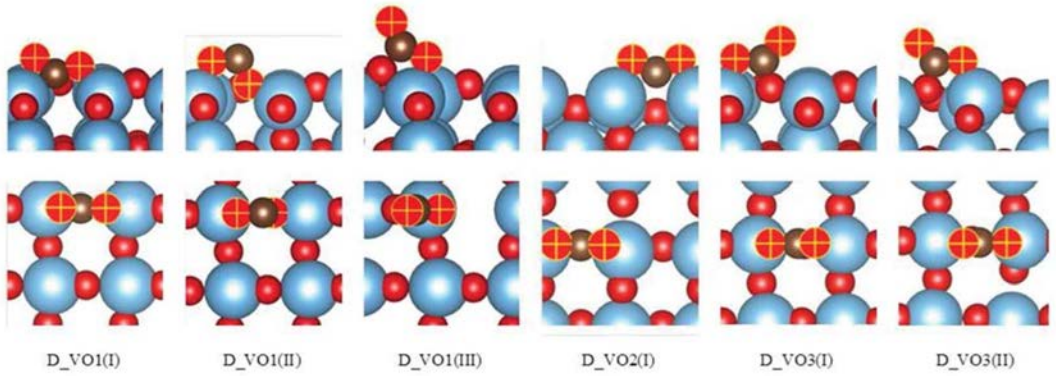

Figure 4. The new adsorption configurations of CO_2 on a reduced anatase (001) surface with different oxygen vacancies, in side view and top view (upper and lower panels, respectively). See text for explanation. (Ti = blue, O_{TiO2} = red, O_{CO2} = red and yellow plus sign, C = brown).

Sites 3 and 4 are equivalent to sites 1 and 2, respectively, but in the neighboring [010] row.

In general, the influence of the oxygen vacancy stays limited compared to the influence found on different TiO_2 surfaces. The adsorption energy does not change more than 5 kcal/mol for the bent configuration, and it changes by about 2 kcal/mol for the physisorbed configurations. Also, the presence of the vacancy does not lead to additional charge transfer, and the bond length and red shift also stay very similar. In contrast, on the anatase (101) surface, it was found in the literature that, for the bent configuration, the adsorption energy changes by up to 13 kcal/mol and, for the physisorbed configuration, it changes by up to 4.5 kcal/mol.[21]

Only for the V_{O1} vacancy, a strong influence is found for the B(I) configuration, and this only occurs when the oxygen vacancy is present in the same [010] row and neighboring the Ti−O(2f)−Ti bridge at which CO_2 is adsorbed. In this case a strong destabilization of the binding configuration is found. The adsorption energy increases from −32.8 kcal/mol on the fully oxidized surface to 1.1 kcal/mol on the reduced anatase (001) facet. The destabilization originates from both electronic and structural causes. The electronic destabilization occurs due to the binding of the Lewis base centers of CO_2, i.e., the oxygen atoms, directly to the Lewis base centers of the surface (i.e., Ti^{3+}), which are generated upon the introduction of an oxygen vacancy. Moreover, the carbon, the Lewis acid center, is not directly bonded to the Ti^{3+} centers, thus not leading to any stabilization of the adsorbed configurations.

Apart from this first electronic contribution, we expect the largest part of the destabilization to originate from the relaxation of the surface, which occurs after the formation of the V_{O1} oxygen vacancy, and which is counteracted by the adsorbed CO_2 molecule. The Ti−O(2f)−Ti angle is 145.6° for the stoichiometric surface and becomes 102.8° upon reduction for the Ti−O(2f)−Ti moiety located in the same [010] row as the oxygen vacancy. Once CO_2 adsorbs, this angle increases to 167.1° for B(I) located above the Ti−O(2f)−Ti bridge neighboring the oxygen vacancy, thus introducing stress on the surface and thereby destabilizing the adsorption configuration.

The generally small influence of the reduction of the surface on the adsorption configurations of the stoichiometric surface compared to the generally larger influence as found on the anatase (101) surface by Sorescu et al.[21] can be explained by the inherent difference in Lewis acidity and basicity of both surfaces. As mentioned above, Mino et al.[19,20] performed combined FTIR and DFT studies on the adsorption of CO and CO_2 on anatase (001) and (101) facets. They concluded that on the (001) facet the Lewis acidity of the Ti-centers is lower compared to the (101) facet, as indicated by the strong bonding of the Ti-cations with the O(2f) anions, resulting in a more screened electrostatic potential. The Lewis basicity of the surface oxygen sites, on the other hand, is higher on the (001) facet, as indicated by the upshift of the valence band characterized by the O 2sp states with the main contribution coming from the O(2f) sites.

In the study of Sorescu, it is found that on the stoichiometric anatase (101) surface CO_2 preferentially adsorbs in a nearly gas phase structure, Sorescu-L(I) (E_{ads} = −11.1 kcal/mol), while the bent configurations, Sorescu-B(I) (E_{ads} = −3.7 kcal/mol) and Sorescu-B(II) (E_{ads} = −0.3 kcal/mol), are unfavorable, as a result of the lower Lewis basicity of the surface oxygens

DOI: 10.1021/acs.jpcc.6b07459
J. Phys. Chem. C 2016, 120, 21659−21669

Table 2. Adsorption Properties of CO_2 on the Reduced TiO_2 Anatase (001) Surfaces with Different Oxygen Vacancies[a]

Configuration	r(Ti−O) (Å)	r(Os−C) (Å)	r(C−O) (Å)	α(OCO) (deg)	E_{ads} (kcal/mol)	υ(CO_2) (cm^{-1})				Δq(CO_2)/|e|
Gas phase			1.177, 1.177	180.0		2365	1316	632	631	
D_VO1(I)	2.075, 1.973		1.272, 1.286	125.1	−48.65	1503	1256	767	455	−0.338
D_VO1(II)	1.971, 2.642, 1.880		1.289, 1.346	108.9	−25.25	1207	928	728	363	−0.422
D_VO1(III)	2.016	1.472	1.200, 1.300	134.7	−1.64	1852	1113	740	714	−0.228
D_VO2(I)	2.008, 1.994		1.265, 1.270	126.1	−25.50	1577	1235	757	469	−0.314
D_VO3(I)	1.932	1.365	1.218, 1.335	128.6	−24.12	1734	1128	824	739	−0.256
D_VO3(II)	1.905	1.366	1.213, 1.347	126.9	−23.56	1754	1082	825	729	−0.252

[a]The bond lengths between Ti and O of CO_2, r(Ti−O_{CO2}), between the surface O and C, r(Os−C), and between C and O of carbon, r(C−O), the bond angle of CO_2, α(OCO), the adsorption energy, vibrational frequencies υ(CO_2), and the charge transfer from the surface to CO_2, Δq(CO_2)/|e|.

compared to anatase (001).[21] If then an oxygen vacancy is introduced in the surface, new Lewis base centers are introduced, causing a significant stabilization of the Sorescu-B(II) configuration (E_{ads} = −16 kcal/mol), which has a comparable structure to the B(I) configuration on the anatase (001) surface. However, on the anatase (001) surface the monodentated carbonate-like structure B(I) is very stable (E_{ads} = −32.8 kcal/mol). This stronger interaction is due to the stronger Lewis basicity of the O(2f) surface oxygens, as also indicated by the greater charge transfer of −0.214 au from the surface to CO_2 for B(I) compared to a charge transfer of −0.146 au for Sorescu-B(II). In reality, this difference in charge transfer is likely to be larger, since the charge transfer for Sorescu-B(II) was calculated with the Bader method, while in this paper we employ the Hirshfeld method, and the Bader method tends to give larger charges compared to the Hirshfeld method.[50] The smaller influence of the presence of oxygen vacancies in anatase (001) is thus due to the already large inherent Lewis basicity of anatase (001), and further increasing the Lewis basicity does not lead to a significant change in interaction.

Apart from the possible influence of the reduction of the TiO_2 surface on the original adsorption configurations, new adsorption possibilities also arise on the reduced surfaces. A pictorial view of the newly formed adsorption configurations is shown in Figure 4, and the relevant bond lengths, bond angles, adsorption energies, vibrational frequencies, and charge transfer are given in Table 2.

3.2.2. CO_2 Adsorption at an Oxygen Vacancy. 3.2.2.1. At the Surface Bridging Oxygen Vacancy, V_{O1}. Three new adsorption configurations, D_VO1(I) to D_VO1(III), are found on the reduced surface containing a V_{O1} vacancy (see Figure 4). D_VO1(I) and D_VO1(II) are configurations which arise when an oxygen atom is removed from the surface. D_VO1(I) has an adsorption energy of −48.65 kcal/mol (see Table 2) and has a structure similar to the monodentated carbonate configuration B(I), which had an adsorption energy of −32.8 kcal/mol. However, as opposed to the latter configuration, the carbon is no longer bonded to the surface Lewis base center, O(2f), as this is no longer available, but now binds to the newly formed Lewis base centers, the Ti^{3+} atoms. The strong stabilization is thus caused by the strong interaction of carbon with the metallic centers, and not due to interactions of the CO_2 oxygen atoms with the titanium atoms. A larger charge transfer from the surface to the CO_2 molecule is found for D_VO1(I) than for B(I), i.e., −0.338 au vs −0.214 au, respectively. Almost all this charge is transferred to the carbon atom: we calculate a charge of −0.247 au to be transferred to the carbon compared to the charge located on the carbon atom in the gas phase geometry, while the charge on the oxygen atoms only changes by −0.039 au and −0.052 au. The greater charge transfer to CO_2 and the stronger red shift of the CO_2 vibrations in D_VO1(I) compared to B(I) indicates a better activation of the CO_2 molecule for CO_2 splitting. However, the C−O bond lengths do not change significantly (cf. Table 1 and Table 2). Pipornpong et al. reported a similar structure on the reduced anatase (001) surface, denoted as CO_2/[TiO2+Vo]-C′ in their publication.[49] They found an adsorption energy of −93.74 kcal/mol for their adsorption configuration, which is much larger than the −48.65 kcal/mol reported in this work. We suspect that this significant difference might be caused by their use of frozen clusters. These frozen clusters do not allow relaxation of the surface when the oxygen vacancy is created, which causes a structure that is significantly less stable and therefore increases the adsorption energy, as the adsorption of CO_2 will release a significant part of the stress in the structure.

The D_VO1(II) configuration (see Figure 4) is an adsorption configuration in which CO_2 is bent and one oxygen is located on the position where a surface oxygen atom was removed to create the vacancy. The adsorption energy is −25.25 kcal/mol (see Table 2). A strong charge transfer is noticeable to the carbon atom, caused by the weakened interaction with the oxygen located at the oxygen vacancy site, as this oxygen now fills the oxygen vacancy. The C−O bond length is increased from 1.177 Å in the gas phase to 1.346 Å for the oxygen located at the oxygen vacancy site and to 1.289 Å for the oxygen located above the Ti^{3+} site. The total charge transfer to CO_2 is −0.422 au, which is larger than for any previously discussed adsorption configuration. Most of this transferred charge is located on the carbon atom with a change of −0.286 au compared to the gas phase structure. In this configuration, a strong red shift is again found, from 2365 to 1207 cm^{-1}. The longer C−O bonds, the strong red shift, and the significant charge transfer indicate the strongest activation of CO_2 reduction to CO thus far.

The last configuration that was found to be stable on the anatase (001) surface containing a surface oxygen vacancy is D_VO1(III) (see Figure 4). We have also tried obtaining this configuration on the stoichiometric surface. However, we find it spontaneously converts to B(I). Only when located near the surface oxygen vacancy is this configuration found to be stable. The adsorption configuration is −1.64 kcal/mol (see Table 2). As this configuration is only slightly stable, we expect it to convert to either B(I) or D_VO1(I), or else desorption will occur and not contribute significantly to the reactivity of anatase (001) with respect to reduction of CO_2. The C−O bonds are less activated than in the other obtained configurations. In particular, we find a smaller red shift of the

DOI: 10.1021/acs.jpcc.6b07459
J. Phys. Chem. C 2016, 120, 21659−21669

Table 3. Adsorption Energies on the Stoichiometric and Reduced Surfaces at Absolute Zero, 300 K, and 400 K in kcal/mol[a]

	Absolute zero					300 K					400 K				
	site 0	site 1	site 2	site 3	site 4	site 0	site 1	site 2	site 3	site 4	site 0	site 1	site 2	site 3	site 4
V_{O1}															
B(I)	-32.82		1.08	-28.16	-34.27	-22.88		11.62	-17.06	-23.18	-19.46	0.00	15.36	-13.01	-19.14
L(I)	-7.31	-5.19	-6.75	-5.19	-6.75	1.43	3.84	1.36	3.84	1.36	4.15	6.85	3.86	6.85	3.86
L(II)	-6.19	-8.01	-6.30	-5.06	-6.67	3.65	0.72	3.58	2.98	3.25	6.98	3.47	6.92	5.49	6.61
L(III)	-4.34	-7.09	-7.09	-7.09	-7.09	4.24	2.74	2.74	2.74	2.74	7.07	6.06	6.06	6.06	6.06
V_{O2}															
B(I)	-32.82	-32.96	32.96			-22.88	-22.70	-22.70			-19.46	-19.11	-19.11		
L(I)	-7.31	-7.30	7.10			1.43	2.27	1.39			4.15	5.48	4.02		
L(II)	-6.19	-5.46	7.69			3.65	4.24	2.30			6.98	7.51	5.69		
L(III)	-4.34		5.00			4.24		4.09			7.07	0.00	7.09		
V_{O3}															
B(I)	-32.82	-30.85	-30.85	-32.64	-32.64	-22.88	-19.86	-19.86	-23.83	-23.83	-19.46	-15.87	-15.87	-20.87	-20.87
L(I)	-7.31	-7.39	-7.39	-7.39	-7.39	1.43	0.33	0.33	0.33	0.33	4.15	2.70	2.70	2.70	2.70
L(II)	-6.19	-4.19	-4.73	-5.60	-6.96	3.65	3.09	4.92	4.04	2.88	6.98	5.29	8.18	7.29	6.20
L(III)	-4.34	-3.98	-4.72	-3.98	-4.72	4.24	2.99	4.09	2.99	4.09	7.07	5.04	7.00	5.04	7.00
D_VO1(I)	-48.65					-37.54					-33.63				
D_VO1(II)	-25.25					-14.98					-11.42				
D_VO1(III)	-1.64					8.51					11.98				
D_VO2(I)	-25.50					-14.14					-10.10				
D_VO3(I)	-24.12					-13.58					-9.84				
D_VO3(II)	-23.56					-12.78					-8.87				

[a]The endothermic and endergonic adsorption configurations are given in red.

asymmetric stretch, shorter C−O bonds, and a smaller charge transfer compared to the other chemisorbed configurations.

We have tried to reproduce the structure CO_2/[TiO2+Vo]-C of Pipornpong et al.[49] In this nondissociative adsorption configuration, the oxygen vacancy is filled with one of the oxygen atoms of CO_2, and CO_2 is oriented in a similar manner as D_VO1(III). However, we found that this configuration is not stable and spontaneously converts to D_VO1(I). Possibly, Pipornpong et al. found this structure to be stable as the result of their frozen cluster approach, which can erroneously create an energy barrier between these two configurations.

3.2.2.2. At the First Subsurface Oxygen Vacancy, V_{O2}. One new adsorption configuration, D_VO2(I), is found on the reduced surface containing a V_{O2} oxygen vacancy. In this configuration, CO_2 takes on a bent configuration and is very comparable to the D_VO1(I) configuration (see Figure 4). However, the CO_2 in this case is bonded to two Ti^{3+} atoms located in the same [100] row as opposed to the same [010] row. The adsorption energy for the D_VO2(I) configuration is −25.50 kcal/mol (see Table 2), which is significantly lower than the −32.96 kcal/mol found for the monodentated carbonate-like structure B(I) if a V_{O2} vacancy is present in the vicinity of the adsorbed CO_2 molecule. However, just as is the case for the D_VO1(I) configuration, a larger charge transfer to CO_2 is found compared to the B(I) configurations. In view of this larger charge transfer and the comparable red shift of the CO_2 vibrations (see Table 3), we expect a greater activation of CO_2 in this bonding configuration.

3.2.2.3. At the Second Subsurface Oxygen Vacancy, V_{O3}. When a V_{O3} oxygen vacancy is present, we find two new monodentated carbonate configurations on the anatase (001) surface. The only difference between the two configurations is their orientation relative to the oxygen vacancy. In the D_VO3(I) configuration, the oxygen atom of CO_2 that is bonded to the surface is located above the titanium atom located at the oxygen vacancy site, while in the D_VO3(II) configuration this oxygen is located above the titanium atom in the same [010] row and in the neighboring [100] row. As mentioned before we have tried to create similar configurations on the stoichiometric surface but found these to spontaneously convert to the B(I) configuration, also when V_{O3} is located in the neighboring [010] row. The lower stability of D_VO3(I) and D_VO3(II) compared to the B(I) configuration and the similarity between the three configurations indicates that the D_VO3(I) and D_VO3(II) will easily convert to B(I). Thus, we do not expect a strong activation of the CO_2 molecule for CO_2 dissociation in these configurations. We rather expect that first a conversion of D_VO3(I) and D_VO3(II) to a B(I) configuration or diffusion of the oxygen vacancy creating a V_{O1} or V_{O2} oxygen vacancy takes place, after which further reactions can occur.

3.3. CO_2 Adsorption at 300 K on Anatase (001). At nonzero temperature we find that the CO_2 adsorption is destabilized, reducing the adsorption strength of the chemisorbed configuration from −32.8 kcal/mol at 0 K to −22.9 kcal/mol at 300 K on the fully oxidized surface. The physisorbed configurations become metastable and the adsorption is endothermic with an adsorption energy ranging from 1.4 to 4.2 kcal/mol, maintaining the same order in stability as at absolute zero. The diffusion barriers from the physisorbed configurations to the bent carbonate configuration decrease for the L(I) configuration from 0.8 kcal/mol at 0 K to 0.7 kcal/mol at 300 K, and they increase for L(II) and L(III) with a maximal barrier of 1.8 kcal/mol at 400 K for L(III). The rate constants for the conversion of the physisorbed configuration to the chemisorbed configuration are in the

DOI: 10.1021/acs.jpcc.6b07459
J. Phys. Chem. C 2016, 120, 21659−21669

order of $10^{11} - 10^{12}$ s^{-1}. However, diffusion between adsorption sites for B(I) is unlikely to occur at these temperatures, as the reaction rate equals 8.1×10^{-11} s^{-1} at 300 K. The influence of oxygen vacancies on the adsorption remains similar at elevated temperatures compared to the influence at absolute zero. All adsorption energies at absolute zero, 300 K, and 400 K are given in Table 3.

3.4. CO_2 Dissociation on Anatase (001). *3.4.1. Stoichiometric Anatase (001) Surface.* As previously mentioned, the dissociation of CO_2 on the fully oxidized anatase (001) surface is unlikely to occur without the help of coadsorbates to stabilize the transition state and the reaction products. We find a dissociative adsorption energy of 67.4 kcal/mol. In the dissociation mechanism, as determined using NEB and shown in Figure 5, we start from the B(I) configuration, as this

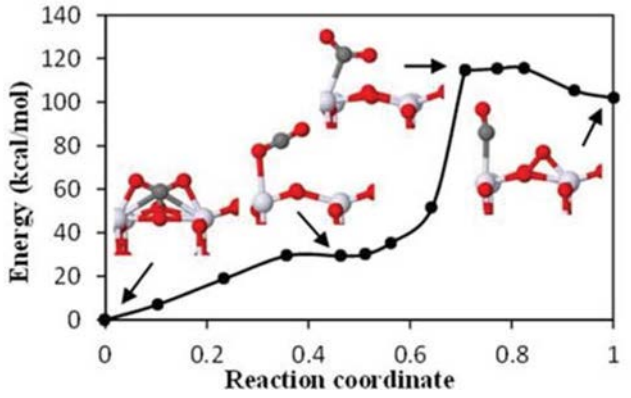

Figure 5. CO_2 dissociation minimal energy pathway starting from B(I) on the stoichiometric anatase (001) surface. No zero-point energy corrections are included in the minimal energy pathway shown.

configuration was shown to be the most promising for CO_2 activation, as inferred from the calculated charge transfer to CO_2, the significant elongation of the C−O bonds, and the red shift in the vibrations. However, we find that B(I) first converts to L(II), which is not activated compared to the gas phase CO_2. The reaction proceeds further through the rotation of the CO_2 molecule, resulting in a transition state with the carbon atom being bonded to Ti and one of the oxygen atoms bonded to O(2f), while maintaining a bent configuration. Subsequently, the C−O bond of the corresponding atoms breaks and CO and O remain adsorbed on the TiO_2 surface. The corresponding energy barrier corrected for the ZPE is 113.6 kcal/mol, and the reaction enthalpy of the dissociation is equal to 98.9 kcal/mol. The corresponding dissociation rate at 300 K is 4.4×10^{-71} s^{-1}. Therefore, this reaction is highly unlikely to occur on the fully oxidized surface, even at elevated temperatures. However, in the previous sections we found that the presence of oxygen vacancies yields newly available adsorption configurations with an apparent higher activation than B(I) and the possibility to stabilize the reaction products by the healing of the vacancy. We shall now discuss the CO_2 dissociation for these new adsorption configurations on the reduced surface.

3.4.2. Reduced Anatase (001) Surface. We here discuss the reaction possibilities and rates for CO_2 dissociation in the presence of the different oxygen vacancies. We exclude the V_{O3} vacancy, as we found that the dissociation reaction would be endothermic by around 50 kcal/mol, and would hence not yield a feasible dissociation possibility. We rather expect that the V_{O3} vacancy will be healed by the diffusion of a surface or subsurface oxygen to the V_{O3} site, thereby creating a V_{O1} or V_{O2} vacancy, respectively.

As starting points for the activation of the dissociation reaction on the reduced anatase (001) surface with a V_{O1} oxygen vacancy, we used three different adsorption configurations, i.e., D_VO1(I), D_VO1(II), and D_VO1(III), for which the minimal energy pathways are shown in Figure 6,

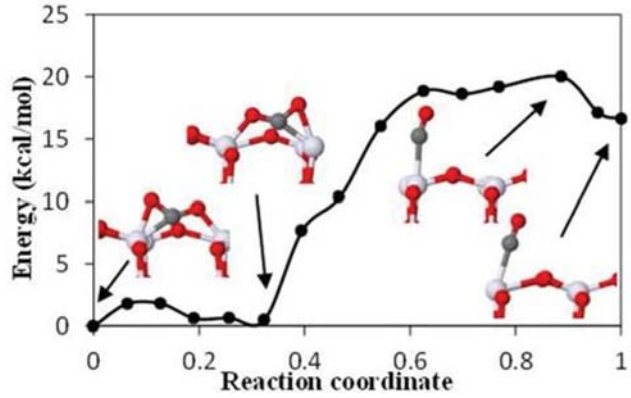

Figure 6. CO_2 dissociation minimal energy pathway starting from D_VO1(I) on the reduced anatase (001) surface. No zero-point energy corrections are included in the minimal energy pathway shown.

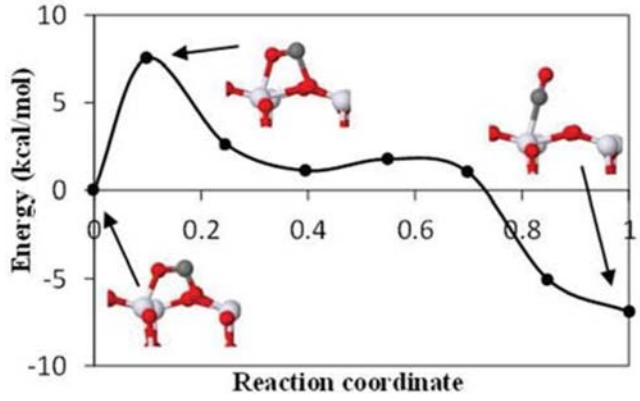

Figure 7. CO_2 dissociation minimal energy pathway starting from D_VO1(II) on the reduced anatase (001) surface. No zero-point energy corrections are included in the minimal energy pathway shown.

Figure 7, and Figure 8, respectively. The reactions all resulted in the oxygen vacancy being healed, similar to the reaction mechanism for CO_2 dissociation on the reduced rutile (110),[51] and the reduced anatase (101).[21] CO is adsorbed on the now fully oxidized surface, with an adsorption energy of −8.3 kcal/mol at absolute zero and −0.06 kcal/mol at 300 K, relative to the gas phase CO and the fully oxidized surface.

For D_VO1(I) (see Figure 6), the minimal energy pathway first crosses a small energy barrier of 1.3 kcal/mol, to yield a minimum which is 0.05 kcal/mol less stable than D_VO1(I). At this minimum, the CO_2 molecule is bonded with its carbon atom to one Ti^{3+} atom and with one of its oxygen atoms to the other Ti^{3+}. The reaction subsequently continues over an energy barrier of 18.1 kcal/mol. At the transition state, we find that CO_2 is already dissociated. The overall reaction is endothermic

DOI: 10.1021/acs.jpcc.6b07459
J. Phys. Chem. C 2016, 120, 21659−21669

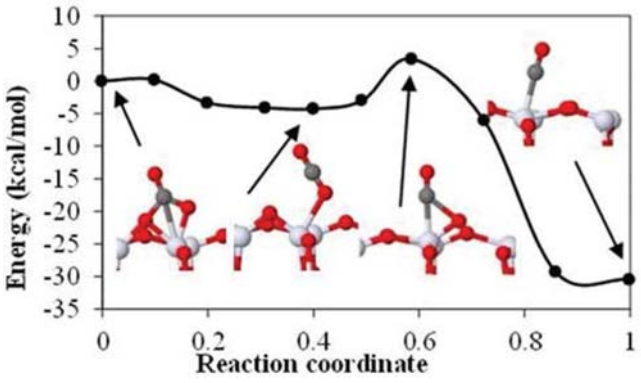

Figure 8. CO_2 dissociation minimal energy pathway starting from D_VO1(III) on the reduced anatase (001) surface. No zero-point energy corrections are included in the minimal energy pathway shown.

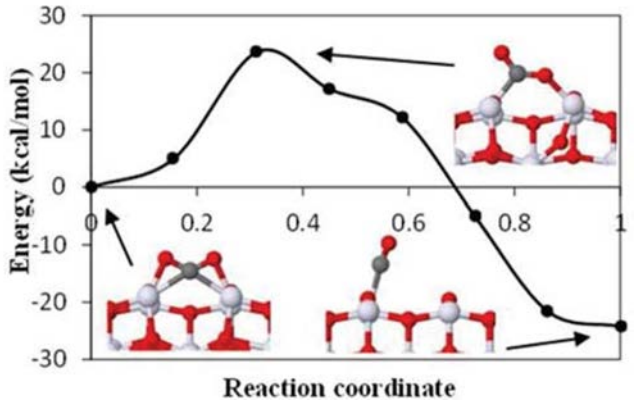

Figure 9. CO_2 dissociation minimal energy pathway starting from D_VO2(I) on the reduced anatase (001) surface. No zero-point energy corrections are included in the minimal energy pathway shown.

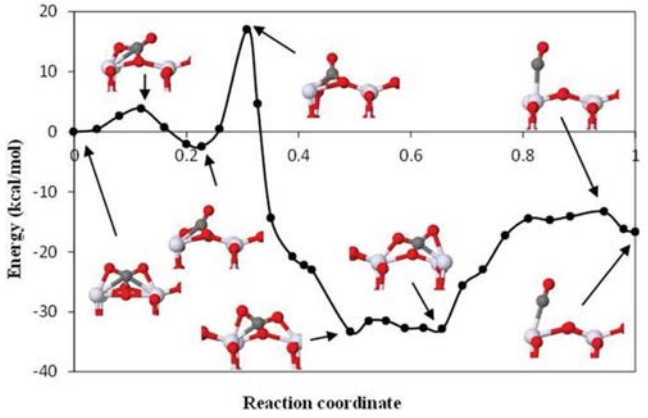

Figure 10. CO_2 dissociation minimal energy pathway starting from B(I) on the reduced anatase (001) surface containing a V_{O2} oxygen vacancy. No zero-point energy corrections are included in the minimal energy pathway shown.

with a corresponding reaction enthalpy (corrected for the ZPE) of 14.9 kcal/mol. As the barrier for the backward reaction at which CO_2 and the oxygen vacancy are recreated is 3.2 kcal/mol and the desorption energy of CO_2 is 0.06 kcal/mol at 300 K, these reactions will be competitive. The reaction rate for dissociation at 300 K is 1.08 s^{-1}.

For D_VO1(II) we find a barrier of 7.3 kcal/mol (see Figure 7). At the transition state, the C−O bond length has increased from 1.35 to 1.83 Å, after which it will convert to an adsorbed CO on the fully oxidized surface. The reaction is exothermic with a reaction enthalpy of −6.4 kcal/mol. The equilibrium constant at 300 K is equal to 1.0×10^5, with a dissociation rate of 5.44×10^6 s^{-1}.

We also performed a nudged elastic band calculation for the dissociation pathway of the D_VO1(III) configuration. This configuration had an adsorption energy of only −1.6 kcal/mol at absolute zero and 8.5 kcal/mol at 300 K, so it will not significantly contribute to the overall dissociation of CO_2. This configuration first converts to the L(II) configuration with no barrier, after which the CO_2 in the L(II) configuration crosses a barrier of 6.5 kcal/mol. The overall reaction enthalpy is equal to −32.0 kcal/mol, so if a reaction occurs, it is unlikely that the reformation of D_VO1(III) will occur, as the equilibrium constant for dissociation is 6.54×10^{18}. This pathway also shows that once CO_2 is adsorbed in the L(II) configuration, it only has to cross a barrier of 6.5 kcal/mol to dissociate, resulting in a dissociation reaction rate of 9.2×10^5 s^{-1} at 300 K. This reaction is competitive to the conversion of L(II) to B(I), which had a barrier of 0.2 kcal/mol.

As starting points for the activation of the dissociation reaction on the reduced anatase (001) surface with a V_{O2} oxygen vacancy, we used two different adsorption configurations, i.e., D_VO2(I) and B(I) adsorbed with one of the oxygen atoms of CO_2 bonded to one of the Ti^{3+} centers. The corresponding reaction mechanisms are shown in Figure 9 and Figure 10, respectively. Both reactions result in the oxygen vacancy being healed, and CO being adsorbed on the now fully oxidized surface with an adsorption energy of −8.3 kcal/mol at absolute zero and −0.06 kcal/mol at 300 K, relative to the gas phase CO and the fully oxidized surface.

For D_VO2(I) an exothermic dissociation is found. The dissociation of CO_2 follows a rotation of CO_2 crossing a barrier of 22.2 kcal/mol. In the dissociation process, one of the oxygen atoms heals the vacancy and CO stays adsorbed on the resulting stoichiometric surface. The total reaction enthalpy equals −26.3 kcal/mol. For this reaction to occur at a sufficient rate, elevated temperatures are needed. We find the reaction rate to increase from 1.1×10^{-3} s^{-1} to 17 s^{-1} upon increasing the temperature from 300 to 400 K. When this reaction takes place, the backward reaction is not likely to occur as the reaction barrier is 49.5 kcal/mol at 300 K.

The CO_2 in the B(I) configuration on the reduced anatase surface containing a V_{O2} vacancy will first undergo a rotation out of the [010] plane, into the direction of the oxygen vacancy. The first barrier, corresponding to this rotation, is 3.4 kcal/mol, resulting in the formation of an intermediate structure. In this structure, one of the oxygen atoms of CO_2 heals the vacancy, and the resulting $Ti-O_{CO2}$ bond lengths are 2.07 and 2.18 Å. The carbon atom stays bonded to all of the three original oxygen atoms of the B(I) configuration. The reaction pathway continues by the elongation of the C−O bond from the oxygen that is filling the V_{O2} oxygen vacancy. The bond elongates from 1.38 Å in the intermediate structure to 1.74 Å in the transition state. In this process, a barrier of 18.2 kcal/mol needs to be overcome. After healing the oxygen vacancy, the D_VO1(I) configuration is formed, and the dissociation of CO_2 will then occur through the pathway of D_VO1(I). The overall reaction is exothermic, and the reaction enthalpy is equal to −18.9 kcal/mol. The rate limiting step in this reaction mechanism is the elongation of the C−O bond from the oxygen that is filling the

DOI: 10.1021/acs.jpcc.6b07459
J. Phys. Chem. C 2016, 120, 21659−21669

Table 4. Energy Barriers at Absolute Zero, 300 K, and 400 K and Rate Constants for Diffusion and Dissociation at 300 and 400 K[a]

	Start	End	$R_{c,300K}$ (s^{-1})	$R_{c,400K}$ (s^{-1})	ΔG_{300K} (kcal/mol)	ΔG_{400K} (kcal/mol)	ΔE_{elec} (kcal/mol)	$\Delta E_{elect+zpe}$ (kcal/mol)
Diffusion	L(I)	B(I)	2.02×10^{12}	3.69×10^{12}	0.7	0.6	0.8	0.8
	B(I)	L(I)	3.94×10^{-6}	4.61×10^{-1}	25.0	24.3	27.4	26.3
	L(II)	B(I)	1.02×10^{12}	1.14×10^{12}	1.1	1.6	0.4	0.2
	B(I)	L(II)	4.75×10^{-8}	4.07×10^{-3}	27.6	28.0	28.2	26.8
	L(III)	B(I)	2.98×10^{11}	3.32×10^{11}	1.8	2.6	0.2	0.3
	B(I)	L(III)	5.16×10^{-9}	1.06×10^{-3}	28.9	29.1	30.1	28.7
	B(I)	B(I)	8.06×10^{-11}	2.59×10^{-5}	31.4	32.0	31.8	30.4
Dissociation	Dissociated	B(I)	19.7	9.17×10^{3}	15.8	16.4	13.7	14.7
	B(I)	Dissociated	4.39×10^{-71}	2.71×10^{-50}	114.1	114.4	115.5	113.6
V_{O1}	Dissociated	Int. D_VO1(I)	8.04×10^{9}	3.19×10^{10}	4.0	4.4	3.4	3.2
	Int. D_VO1(I)	D_VO1(I)	2.64×10^{12}	6.56×10^{12}	0.5	0.2	1.8	1.2
	Total		8.01×10^{9}	3.18×10^{10}				
	D_VO1(I)	Int. D_VO1(I)	2.34×10^{12}	5.95×10^{12}	0.6	0.3	1.8	1.3
	Int. D_VO1(I)	Dissociated	1.08	3.37×10^{3}	17.5	17.2	19.9	18.1
	Total		1.08	3.37×10^{3}				
	Dissociated	D_VO1(II)	52.3	1.34×10^{4}	15.2	16.1	14.4	13.7
	D_VO1(II)	Dissociated	5.44×10^{6}	1.33×10^{8}	8.3	8.8	7.5	7.3
	Dissociated	Int. D_VO1(III)	1.41×10^{-13}	1.34×10^{-7}	35.2	36.2	33.9	33.6
	Int. D_VO1(III)	D_VO1(III)	1.06×10^{8}	6.43×10^{8}	6.6	7.5	4.5	4.3
	Total		1.41×10^{-13}	1.34×10^{-7}				
	D_VO1(III)	Int. D_VO1(III)	5.54×10^{12}	4.69×10^{12}	0.1	0.5	0.2	-0.6
	Int. D_VO1(III)	Dissociated	9.21×10^{5}	1.25×10^{7}	7.7	10.7	7.7	6.5
	Total		9.21×10^{5}	1.25×10^{7}				
V_{O2}	Dissociated	D_VO2(I)	5.06×10^{-24}	3.10×10^{-15}	49.5	50.2	47.9	48.5
	D_VO2(I)	Dissociated	1.10×10^{-3}	17.2	21.6	21.4	23.6	22.2
	Dissociated	Int. D_VO1(I)	8.04×10^{9}	3.19×10^{10}	4.0	4.4	3.4	3.2
	Int. D_VO1(I)	D_VO1(I)	2.64×10^{12}	6.56×10^{12}	0.5	0.2	1.8	1.2
	D_VO1(I)	Int. B(I)	2.24×10^{-24}	2.00×10^{-15}	50.0	50.6	49.0	49.3
	Int. B(I)	B(I)	1.01×10^{8}	1.43×10^{9}	6.6	6.9	6.3	6.1
	Total		2.24×10^{-24}	2.00×10^{-15}				
	B(I)	Int. B(I)	4.2×10^{9}	1.85×10^{10}	4.3	4.9	3.9	3.4
	Int. B(I)	D_VO1(I)	3.77×10^{-1}	9.93×10^{2}	18.1	18.2	19.5	18.2
	D_VO1(I)	Int. D_VO1(I)	2.34×10^{12}	5.95×10^{12}	0.6	0.3	1.8	1.3
	Int. D_VO1(I)	Dissociated	1.08	3.37×10^{3}	17.5	17.2	19.9	18.1
	Total		2.79×10^{-1}	7.67×10^{2}				

[a]The cells for conversion of the physisorbed states to the chemisorbed B(I) configuration are shown in gray, and the backward reaction in orange. For the dissociation, the cells corresponding to the reaction from the dissociated state to the adsorbed CO_2 configurations are given in gray, and the dissociation is given in orange. The rates below 1 s^{-1} are given in red. In this table, Int. is the contraction of intermediate.

V_{O2} oxygen vacancy, causing the reaction rate to drop to 0.28 s^{-1} at 300 K, which increases to 7.7×10^2 s^{-1} at 400 K.

All energy barriers at absolute zero, 300 and 400 K and all rate constants for diffusion and dissociation at 300 and 400 K are given in Table 4.

4. CONCLUSION

We have studied the adsorption of CO_2 and the activation for CO_2 dissociation on the fully oxidized and reduced anatase (001) surfaces using density functional theory calculations with long-range dispersion energy corrections. On the fully oxidized surface we identified four different adsorption configurations for CO_2: One strongly chemisorbed bent configuration, B(I), and three linear physisorbed configurations, L(I)−L(III), which almost retain their gas phase properties. We also studied the influence of the introduction of different oxygen vacancies on the aforementioned adsorption configurations. The influence of the different vacancies on the adsorption configurations found on the stoichiometric surface remains limited, except when the CO_2 is adsorbed in the B(I) configuration on top of the Ti−O(2f)−Ti moiety neighboring a V_{O1} oxygen vacancy in the same [010] row. This configuration is strongly destabilized through the counteraction of the relaxation of the surface after formation of the vacancy, and the interaction of Lewis base centers. New adsorption configurations originate from the presence of oxygen vacancies in the anatase (001) surface. For the different oxygen vacancies, we found a total of six new bent adsorption configurations. Just as with the B(I) configuration, significant charge transfer to CO_2, large vibrational red shifts, and sizable elongations of the C−O bonds indicate a substantial bond weakening for these newly formed adsorption configurations. For D_VO1(III), D_VO3(I), and D_VO3(II) we found a smaller red shift than for B(I). CO_2 dissociation on a fully oxidized anatase (001) surface starting from the B(I) adsorption configuration is unlikely to occur, as the corresponding barrier equals 113.6 kcal/mol. In the presence of the V_{O3} vacancy, we found that the reaction is endothermic with at least 45 kcal/mol, and hence also unlikely to happen. However, we found significantly lower reaction barriers in the presence of the other oxygen vacancies, as these vacancies provide a means of stabilizing the end products, by using one of the oxygen atoms of the CO_2 molecule to heal the oxygen

DOI: 10.1021/acs.jpcc.6b07459
J. Phys. Chem. C 2016, 120, 21659−21669

vacancy. As D_VO1(III) converts to L(II) without a barrier and the barrier for dissociation starting from the physisorbed configuration is 6.54 kcal/mol, direct dissociation after physisorption is competitive with the conversion of the physisorbed configuration to the bent monodentated carbonate-like structure B(I). All dissociations starting from different adsorption configurations, except for the D_VO1(I) configuration, on the reduced surfaces are exothermic. The end product for all these reaction pathways is a CO molecule being adsorbed on the fully oxidized surface with an adsorption energy of −8.3 kcal/mol with respect to the gas phase CO and the fully oxidized surface. The results of this study show that oxygen vacancies play a significant role in the dissociation of CO_2 on the anatase (001) surface, and thus we anticipate they will play an important role in complex problems, such as the conversion of CO_2 to value-added chemicals.

AUTHOR INFORMATION

Corresponding Author

*Tel: +32-3-265.23.88. Fax: +32-3-265.23.43. E-mail: erik.neyts@uantwerpen.be.

Notes

The authors declare no competing financial interest.

ACKNOWLEDGMENTS

Stijn Huygh is funded as an aspirant of the Research Foundation Flanders (FWO, project number 11C0115N). This work was carried out using the Turing HPC infrastructure at the CalcUA core facility of the Universiteit Antwerpen (UAntwerpen), a division of the Flemish Supercomputer Center VSC, funded by the Hercules Foundation, the Flemish Government (department EWI), and the UAntwerpen.

REFERENCES

(1) IPCC. *Climate Change 2014: Synthesis Report*; 2014.

(2) IPCC. *Climate Change 2007: Synthesis Report*; 2007.

(3) Oreskes, N. The Scientific Consensus on Climate Change. *Science* **2005**, *306*, 2004−2005.

(4) Balzani, V.; Credi, A.; Venturi, M. Photochemical Conversion of Solar Energy. *ChemSusChem* **2008**, *1*, 26−58.

(5) National oceanic and atmospheric administration. http://www.esrl.noaa.gov/gmd/ccgg/trends/global.html (accessed May 22, 2015).

(6) Snoeckx, R.; Heijkers, S.; Van Wesenbeeck, K.; Lenaerts, S.; Bogaerts, A. CO_2 Conversion in a Dielectric Barrier Discharge Plasma: N_2 in the Mix as a Helping Hand or Problematic Impurity? *Energy Environ. Sci.* **2016**, *9*, 999−1011.

(7) Bogaerts, A.; Kozak, T.; van Laer, K.; Snoeckx, R. Plasma-Based Conversion of CO_2: Current Status and Future Challenges. *Faraday Discuss.* **2015**, *183*, 217−232.

(8) Ramakers, M.; Michielsen, I.; Aerts, R.; Meynen, V.; Bogaerts, A. Effect of Argon or Helium on the CO_2 Conversion in a Dielectric Barrier Discharge. *Plasma Processes Polym.* **2015**, *12*, 755−763.

(9) Aerts, R.; Martens, T.; Bogaerts, A. Influence of Vibrational States on CO_2 Splitting by Dielectric Barrier Discharges. *J. Phys. Chem. C* **2012**, *116*, 23257−23273.

(10) Aerts, R.; Somers, W.; Bogaerts, A. Carbon Dioxide Splitting in a Dielectric Barrier Discharge Plasma: A Combined Experimental and Computational Study. *ChemSusChem* **2015**, *8*, 702−716.

(11) Paulussen, S.; Verheyde, B.; Tu, X.; Bie, C.; De Martens, T.; Petrovic, D.; Bogaerts, A.; Sels, B. Conversion of Carbon Dioxide to Value-Added Chemicals in Atmospheric Pressure Dielectric Barrier Discharges. *Plasma Sources Sci. Technol.* **2010**, *19*, 34015.

(12) Neyts, E. C.; Bogaerts, A. Understanding Plasma Catalysis through Modelling and Simulation-a Review. *J. Phys. D: Appl. Phys.* **2014**, *47*, 224010.

(13) Neyts, E. C.; Ostrikov, K.; Sunkara, M. K.; Bogaerts, A. Plasma Catalysis: Synergistic Effects at the Nanoscale. *Chem. Rev.* **2015**, *115*, 13408−13446.

(14) D'Alessandro, D. M.; Smit, B.; Long, J. R. Carbon Dioxide Capture: Prospects for New Materials. *Angew. Chem., Int. Ed.* **2010**, *49*, 6058−6082.

(15) Inoue, T.; Fujishima, A.; Konishi, S.; Honda, K. Photoelectrocatalytic Reduction of Carbon Dioxide in Aqueous Suspensions of Semiconductor Powders. *Nature* **1979**, *277*, 637−638.

(16) Yu, J.; Low, J.; Xiao, W.; Zhou, P.; Jaroniec, M. Enhanced Photocatalytic CO_2-Reduction Activity of Anatase TiO_2 by Coexposed {001} and {101} Facets. *J. Am. Chem. Soc.* **2014**, *136*, 8839−8842.

(17) Onal, I.; Soyer, S.; Senkan, S. Adsorption of Water and Ammonia on TiO_2-Anatase Cluster Models. *Surf. Sci.* **2006**, *600*, 2457−2469.

(18) Vittadini, A.; Selloni, A.; Rotzinger, F. P.; Grätzel, M. Structure and Energetics of Water Adsorbed at TiO_2 Anatase (101) and (001) Surfaces. *Phys. Rev. Lett.* **1998**, *81*, 2954−2957.

(19) Mino, L.; Ferrari, A. M.; Lacivita, V.; Spoto, G.; Bordiga, S.; Zecchina, A. CO Adsorption on Anatase Nanocrystals: A Combined Experimental and Periodic DFT Study. *J. Phys. Chem. C* **2011**, *115*, 7694−7700.

(20) Mino, L.; Spoto, G.; Ferrari, A. M. CO_2 Capture by TiO_2 Anatase Surfaces: A Combined DFT and FTIR Study. *J. Phys. Chem. C* **2014**, *118*, 25016−25026.

(21) Sorescu, D. C.; Al-Saidi, W. A.; Jordan, K. D. CO_2 Adsorption on TiO_2(101) Anatase: A Dispersion-Corrected Density Functional Theory Study. *J. Chem. Phys.* **2011**, *135*, 124701.

(22) Metiu, H.; Chrétien, S.; Hu, Z.; Li, B.; Sun, X. Chemistry of Lewis Acid-Base Pairs on Oxide Surfaces. *J. Phys. Chem. C* **2012**, *116*, 10439−10450.

(23) Sorescu, D. C.; Lee, J.; Al-Saidi, W. A.; Jordan, K. D. CO_2 Adsorption on TiO_2(110) Rutile: Insight from Dispersion-Corrected Density Functional Theory Calculations and Scanning Tunneling Microscopy Experiments. *J. Chem. Phys.* **2011**, *134*, 104707.

(24) Wang, Y.; Sun, H.; Tan, S.; Feng, H.; Cheng, Z.; Zhao, J.; Zhao, A.; Wang, B.; Luo, Y.; Yang, J.; et al. Role of Point Defects on the Reactivity of Reconstructed Anatase Titanium Dioxide (001) Surface. *Nat. Commun.* **2013**, *4*, 2214.

(25) Aschauer, U.; He, Y.; Cheng, H.; Li, S. C.; Diebold, U.; Selloni, A. Influence of Subsurface Defects on the Surface Reactivity of TiO_2: Water on Anatase (101). *J. Phys. Chem. C* **2010**, *114*, 1278−1284.

(26) Aschauer, U.; Chen, J.; Selloni, A. Peroxide and Superoxide States of Adsorbed O_2 on Anatase TiO_2 (101) with Subsurface Defects. *Phys. Chem. Chem. Phys.* **2010**, *12*, 12956−12960.

(27) Huygh, S.; Neyts, E. C. Adsorption of C and CH_x Radicals on Anatase (001) and the Influence of Oxygen Vacancies. *J. Phys. Chem. C* **2015**, *119*, 4908−4921.

(28) Barzan, C.; Groppo, E.; Bordiga, S.; Zecchina, A. Defect Sites in H_2-Reduced TiO_2 Convert Ethylene to High Density Polyethylene without Activator. *ACS Catal.* **2014**, *4*, 986−989.

(29) Liu, L.; Jiang, Y.; Zhao, H.; Chen, J.; Cheng, J.; Yang, K.; Li, Y. Engineering Coexposed {001} and {101} Facets in Oxygen-Deficient TiO_2 Nanocrystals for Enhanced CO_2 Photoreduction under Visible Light. *ACS Catal.* **2016**, *6*, 1097−1108.

(30) Ramesha, G. K.; Brennecke, J. F.; Kamat, P. V. Origin of Catalytic Effect in the Reduction of CO_2 at Nanostructured TiO_2 Films. *ACS Catal.* **2014**, *4*, 3249−3254.

(31) Scheiber, P.; Fidler, M.; Dulub, O.; Schmid, M.; Diebold, U.; Hou, W.; Aschauer, U.; Selloni, A. Sub)Surface Mobility of Oxygen Vacancies at the TiO_2 Anatase (101) Surface. *Phys. Rev. Lett.* **2012**, *109*, 136103.

(32) Cheng, H.; Selloni, A. Surface and Subsurface Oxygen Vacancies in Anatase TiO_2 and Differences with Rutile. *Phys. Rev. B: Condens. Matter Mater. Phys.* **2009**, *79*, 2−5.

(33) Huygh, S.; Bogaerts, A.; van Duin, A. C. T.; Neyts, E. C. Development of a ReaxFF Reactive Force Field for Intrinsic Point Defects in Titanium Dioxide. *Comput. Mater. Sci.* **2014**, *95*, 579−591.

DOI: 10.1021/acs.jpcc.6b07459
J. Phys. Chem. C 2016, 120, 21659−21669

(34) Kresse, G.; Furthmüller, J. Efficiency of Ab-Initio Total Energy Calculations for Metals and Semiconductors Using a Plane-Wave Basis Set. *Comput. Mater. Sci.* **1996**, *6*, 15−50.
(35) Kresse, G.; Furthmuller, J. Efficient Iterative Schemes for Ab Initio Total-Energy Calculations Using a Plane-Wave Basis Set. *Phys. Rev. B: Condens. Matter Mater. Phys.* **1996**, *54*, 11169−11186.
(36) Perdew, J.; Burke, K.; Ernzerhof, M. Generalized Gradient Approximation Made Simple. *Phys. Rev. Lett.* **1996**, *77*, 3865−3868.
(37) Blöchl, P. E. Projector Augmented-Wave Method. *Phys. Rev. B: Condens. Matter Mater. Phys.* **1994**, *50*, 17953−17979.
(38) Tkatchenko, A.; Scheffler, M. Accurate Molecular van Der Waals Interactions from Ground-State Electron Density and Free-Atom Reference Data. *Phys. Rev. Lett.* **2009**, *102*, 073005.
(39) Al-Saidi, W. A.; Voora, V. K.; Jordan, K. D. An Assessment of the vdW-TS Method for Extended Systems. *J. Chem. Theory Comput.* **2012**, *8*, 1503−1513.
(40) Ghysels, A.; Verstraelen, T.; Hemelsoet, K.; Waroquier, M.; Van Speybroeck, V. TAMkin: A Versatile Package for Vibrational Analysis and Chemical Kinetics. *J. Chem. Inf. Model.* **2010**, *50*, 1736−1750.
(41) Hirshfeld, F. L. Bonded-Atom Fragments for Describing Molecular Charge Densities. *Theor. Chim. Acta* **1977**, *44*, 129−138.
(42) Sheppard, D.; Xiao, P.; Chemelewski, W.; Johnson, D. D.; Henkelman, G. A Generalized Solid-State Nudged Elastic Band Method. *J. Chem. Phys.* **2012**, *136*, 136.
(43) Sheppard, D.; Henkelman, G. Paths to Which the Nudged Elastic Band Converges. *J. Comput. Chem.* **2011**, *32*, 1769−1771.
(44) Sheppard, D.; Terrell, R.; Henkelman, G. Optimization Methods for Finding Minimum Energy Paths. *J. Chem. Phys.* **2008**, *128*, 134106.
(45) Henkelman, G.; Uberuaga, B. P.; Jónsson, H. Climbing Image Nudged Elastic Band Method for Finding Saddle Points and Minimum Energy Paths. *J. Chem. Phys.* **2000**, *113*, 9901−9904.
(46) Henkelman, G.; Jónsson, H. Improved Tangent Estimate in the Nudged Elastic Band Method for Finding Minimum Energy Paths and Saddle Points. *J. Chem. Phys.* **2000**, *113*, 9978−9985.
(47) Jónsson, H.; Mills, G.; Jacobsen, K. W. Nudged Elastic Band Method for Finding Minimum Energy Paths of Transitions. *Class. Quantum Dyn. Condens. Phase Simulations* **1997**, 385−404.
(48) Indrakanti, V. P.; Kubicki, J. D.; Schobert, H. H. Quantum Chemical Modeling of Ground States of CO_2 Chemisorbed on Anatase (001), (101), and (010) TiO_2 Surfaces. *Energy Fuels* **2008**, *22*, 2611−2618.
(49) Pipornpong, W.; Wanbayor, R.; Ruangpornvisuti, V. Adsorption CO_2 on the Perfect and Oxygen Vacancy Defect Surfaces of Anatase TiO2 and Its Photocatalytic Mechanism of Conversion to CO. *Appl. Surf. Sci.* **2011**, *257*, 10322−10328.
(50) Fonseca Guerra, C.; Handgraaf, J.-W.; Baerends, E. J.; Bickelhaupt, F. M. Voronoi Deformation Density (VDD) Charges: Assessment of the Mulliken, Bader, Hirshfeld, Weinhold, and VDD Methods for Charge Analysis. *J. Comput. Chem.* **2004**, *25*, 189−210.
(51) Lee, J.; Sorescu, D. C.; Deng, X. Electron-Induced Dissociation of CO_2 on TiO_2(110). *J. Am. Chem. Soc.* **2011**, *133*, 10066−10069.

DOI: 10.1021/acs.jpcc.6b07459
J. Phys. Chem. C 2016, 120, 21659−21669